November 23 & 24

COMBURA

NVV 2022

Book of Abstracts

NVV
Nederlandse Vereniging
voor Vlamonderzoek

THE COMBUSTION INSTITUTE
1954

LES STUDY OF SOOT FORMATION IN TURBULENT NON-PREMIXED FLAME WITH SECTIONAL METHOD

Abhijit Kalbhor*, Daniel Mira and Jeroen van Oijen***

a.j.kalbhor@tue.nl

*Eindhoven University of Technology, Eindhoven, the Netherlands

**Barcelona Supercomputing Center, Barcelona, Spain

Abstract

In view of strict emission regulations, the development of sophisticated models describing soot formation and the evolution of its particle size distribution (PSD) is crucial challenge in the design of sustainable combustion devices. However, the formation of soot in turbulent flames, which are often present in such combustion systems, becomes a highly complex physico-chemical process owing to the strong coupling between the turbulent flow field and chemistry. In this context, the formation of soot in turbulent non-premixed flame is investigated using the discrete sectional method (DSM) based soot model and Flamelet Generated Manifold (FGM) chemistry [1] within the LES framework. In the DSM model, soot particle volume is partitioned into a finite number of sections, and the sectional soot mass fraction is transported. The soot formation rates are evaluated through contributions of soot nucleation, PAH condensation, surface growth (by HACA mechanism), oxidation, and coagulation sub-processes [2].

The LES-FGM-DSM framework is applied on the Sandia sooting turbulent non-premixed ethylene/air piloted jet flame [3]. This flame features a burner with a central jet of pure C_2H_4 (at a Reynolds number of 20000 based on the diameter $D = 3.2\,\mathrm{mm}$) and low-speed pilot injection of C_2H_4-air pre-mixture at an equivalence ratio of 0.9. The piloted flame is surrounded by a co-flow of air. The LES computational domain spans $1\,\mathrm{m}\times0.3\,\mathrm{m}\times2\pi$ in axial, radial, and circumferential directions, respectively. The thermochemical state of reacting mixture is parameterized by the mixture fraction Z and the progress variable $\mathcal{Y}$ and their variances. The detailed kinetic scheme KM2 [4] is retained to compute the steady and unsteady 1-D counterflow flamelets with the Unity Lewis diffusion model. Complete soot kinetics with 30 sections is included in the flamelets computations. Sub-grid scale interactions between chemistry and turbulence are modeled using the presumed-PDF approach with β-shaped density function, while soot and sub-grid turbulence interactions are not accounted for in the present formalism. The LES is performed using the Alya code [5] on the HAWK cluster.

The time-averaged field of soot volume fraction f_v is shown in Fig. 1a. As can be seen, soot is restricted to fuel-rich regions within the stoichiometric mixture fraction iso-contour. The radial profiles of mean and RMS of f_v along the different axial heights are compared in Fig. 1b. The qualitative trends in the experimental data are reasonably well reproduced in the simulations, however, the magnitude of the soot volume fraction is underpredicted. The axial profiles of mean and RMS soot volume fraction along the centerline are shown in Fig. 1c. The position of peak f_v is slightly shifted upstream compared to measurements, indicating that the soot consumption is predicted early in comparison to experiments. Furthermore, the time-averaged PSD at different axial locations along the flame centerline are plotted in Fig. 1d. The PSDs feature unimodal to bimodal transition, evident around $z/D = 70$. The number density of larger-sized particles increases during this process as nucleated soot particles grow through surface reactions. Beyond $z/D = 150$, the number density starts to drop due to the soot oxidation accompanied by fuel-lean conditions. In summary, the current LES-FGM-DSM

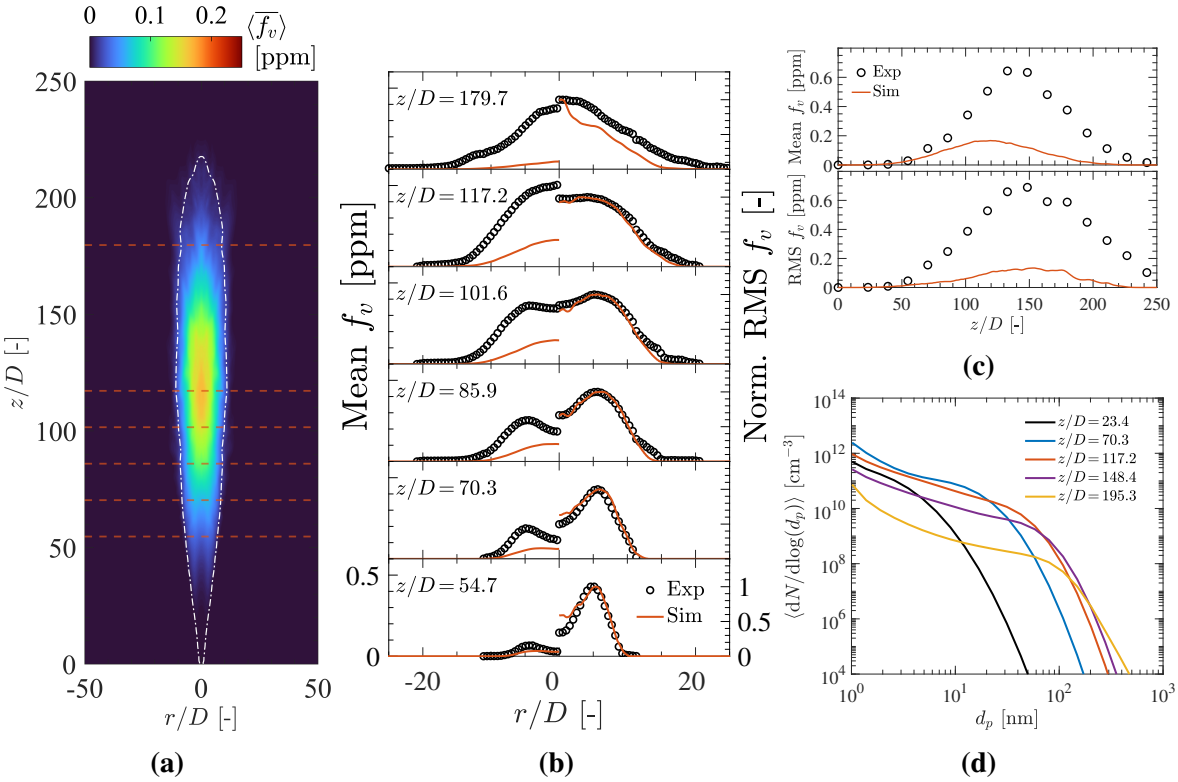

Figure 1. Time-averaged fields of soot volume fraction f_v (a). Comparison between experimental (symbols) and numerical (line) data for mean and RMS of f_v profiles at several axial heights (b) and centerline (c). Soot PSDs at different positions along the centerline (d).

formalism shows a promising comparison with experimental measurements for soot formation in turbulent non-premixed flame by enabling a description of soot PSD. Nevertheless, further modeling improvements are needed concerning the radiative heat transfer, subgrid-scale soot-turbulence interactions, etc, which is left for future investigation.

References

[1] J. van Oijen and L. de Goey, "Modelling of premixed counterflow flames using the flamelet-generated manifold method," *Combust. Theor. Model.*, vol. 6, no. 3, pp. 463–478, 2002.

[2] C. Hoerlle and F. Pereira, "Effects of CO_2 addition on soot formation of ethylene non-premixed flames under oxygen enriched atmospheres," *Combust. Flame*, vol. 203, pp. 407–423, 2019.

[3] J. Zhang, C. R. Shaddix, and R. W. Schefer, "Design of "model-friendly" turbulent non-premixed jet burners for c2+ hydrocarbon fuels," *Rev. Sci. Inst.*, vol. 82, no. 7, p. 074 101, 2011.

[4] Y. Wang, A. Raj, and S. Chung, "A PAH growth mechanism and synergistic effect on PAH formation in counterflow diffusion flames," *Combust. Flame*, vol. 160, no. 9, pp. 1667–1676, 2013.

[5] M. Vázquez *et al.*, "Alya: Multiphysics engineering simulation toward exascale," *J. Comput. Sci.*, vol. 14, pp. 15–27, 2016.

Multi-dimensional Simulations of Iron Particle Combustion in Alya and NTMIX

Swagnik Guhathakurta[1]; Xiaocheng Mi[1]; Benedicte Cuenot[1,2]; Jeroen van Oijen[1]

In recent years, there has been a growing interest in the combustion of metal powders as fuels for renewable energy. Since these particles do not contain carbon, combustion of these particles results in zero carbon-dioxide emissions. The oxidation of metals results in metal oxides which, depending on the type of metal being used, can be collected and reduced back to their original metal form using clean energy. The metal particle of particular interest is iron because of the discrete nature of its combustion, which is unlike most other metals. Due to high boiling point of iron, the particles do not undergo phase change. During combustion, the particle remains in its solid state and thus the reactions happen only at its surface. This enables the oxidized iron particles to be easily collected after combustion. However, there is a con of this discrete flame propagation behavior – numerical modeling of this combustion behavior can be a challenge.

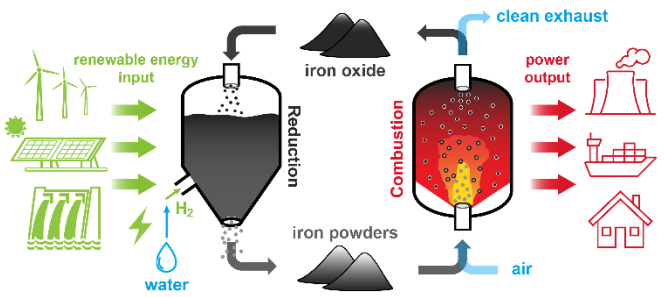

Figure 1 – *Schematic of recyclability of iron powders for energy generation*

For the research presented here, we ran several multidimensional, unsteady numerical simulations of iron particle flame propagation. The simulations solved the reactive Navier-Stokes equations coupled to a Lagrangian granular multiphase model. The combustion and physical models for the particle are based on the work by (Hazenberg, 2021). Two different numerical codes were used for these simulations. Iron flame propagation tests were carried out using the numerical solver Alya (Vázquez, 2016). In these tests, we simulated laminar iron flame propagation in a long three-dimensional rectangular box, with different equivalence ratios. We also performed simulations using another code, NTMIX (VINOT, 2020), in which we investigated the issue of numerical divergence when simulating iron particle combustion in a Direct Numerical Simulation (DNS) code. In order to properly capture the discrete flame propagation behavior of iron flames, the inter-particle gradients need to be resolved. However, when the grid resolution is less than or similar to the particle size, dumping the particle source terms into a single cell in which the point source particle exists, results in numerical divergence. This issue can be remedied by distributing the source terms over a larger number of neighboring cells. This method is known as the Distribution Kernel Method (DKM). We developed two DKM methods – one in which the source terms are distributed uniformly over a finite number of cells, and another in which they are distributed using a gaussian profile.

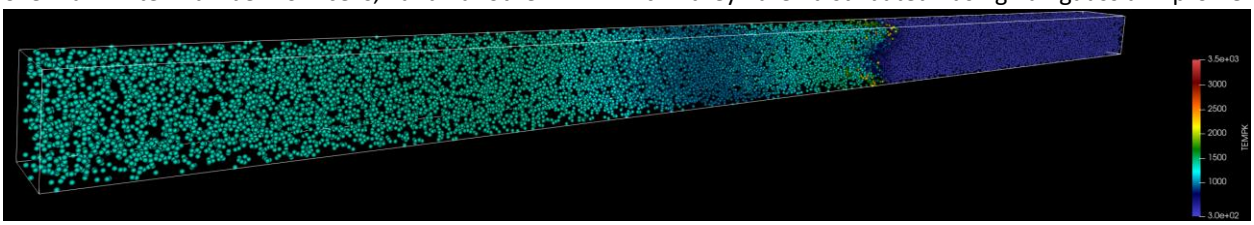

Figure 2 – *3-D iron flame propagation in Alya*

The results from Alya show that getting the flame to propagate can be tricky. The flame propagation is highly dependent on the ignition method and the inter-particle distance. Since the reactions happen only at the surface of the particles, ignition of neighboring particles depends on how far away they are from an ignited particle. If they are too far, then the hot particles move further away along with the expanding hot gases. The heat conduction time is not fast enough to ignite the neighboring particles. For equivalence ratios of one, the flame fails to propagate. For

[1] Mechanical Engineering, Eindhoven University of Technology, Eindhoven, the Netherlands
[2] CERFACS, France

higher equivalence ratios, particles are closer to each other and the flame propagates further. When the equivalence ratio is 1.5, the flame manages to propagate to the end of the channel. Note that the discrete nature of flame propagation is not observed in these cases because the grid resolution is not enough to capture the inter-particle gradients.

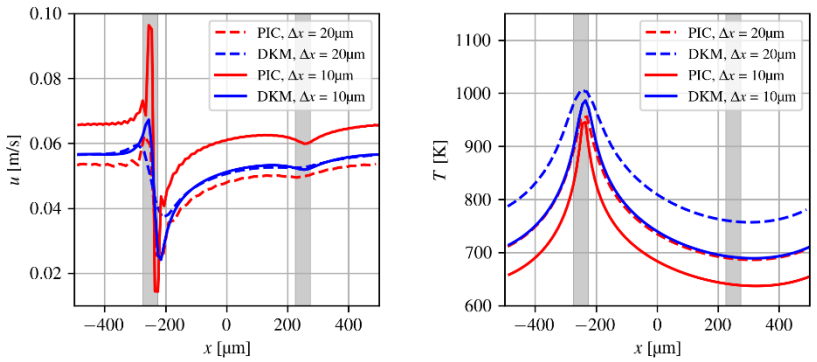

Figure 3 *Left -- x-component of gas velocity and right -- gas temperature in center of domain along the flow direction for different interphase coupling methods at different mesh resolutions; particle locations are indicated in grey*

When the grid resolution is increased such that the cell size is about the same or lesser than the particle size, numerical divergence is observed when the source is only distributed to the local cell. This issue was investigated using NTMIX. This either causes the simulation to stop or gives results that are not physical. If a uniform DKM is used, the simulation do es not stop and there is no divergence. However, the uniform DKM is not the most physically accurate method. Thus, a gaussian distribution DKM was also developed. This distributes the sources over multiple cells in a close neighborhood depending on how far the cells are from the particle. This results in much more accurate data when compared to particle-resolved DNS simulations.

References

Hazenberg, T. &. (2021). Structures and burning velocities of flames in iron aerosols. *Proceedings of the Combustion Institute*, 4383-4390.

Vázquez, M. H.-S. (2016). Alya: Multiphysics engineering simulation toward exascale. *Journal of computational science*, 15-27.

VINOT, B. E. (2020). Retrieved from cerfacs.fr: https://cerfacs.fr/wp-content/uploads/2020/09/VINOT-WN2020.pdf

NOx EMISSIONS TRENDS IN HYDROGEN LEAN PREMIXED FLAMELETS AT HIGH STRAIN RATE

A. Porcarelli*, B. Kruljevic* and I. Langella*
a.porcarelli@tudelft.nl
*TU Delft, Faculty of Aerospace Engineering, Flight Performance & Propulsion group, Kluyverweg 1, 2629 HS Delft, Netherlands

Abstract

NOx formation in lean premixed and highly-strained pure hydrogen-air flamelets is investigated numerically. Detailed-chemistry, one-dimensional and two-dimensional simulations are performed on a reactants-to-products counter-flow configuration with varying applied strain rate. Both solutions show a decreasing NOx trend as the applied strain rate is increased. This decreasing emission outcome is highlighted in this study for lean pure-hydrogen flamelets. Furthermore, a detailed analysis of the NOx formation pathways shows that the most significant decrease is observed along the thermal NOx route.

Introduction

One interesting property of hydrogen flames that has not been fully understood yet is its behaviour under strain. Hydrogen addition has been shown to delay the extinction strain rate [1], proving that hydrogen is able to sustain very high strain rates. It has also been shown for syngas fuels that hydrogen percentage influences the lean flame response with strain in terms of flame temperature and NOx emissions and consumption speed [2,3]. In particular, in lean conditions the consumption speed is shown to increase with strain, and this trend is opposite to the one observed for hydrocarbon flames [4]. Furthermore, the hydrogen-enhanced differential diffusion effects and the strain sensitivity have been proved to be interdependent [5]. Even more interestingly, while the mass burning rate decreases with strain for methane flames, the opposite trend is observed for hydrogen flames, particularly in lean conditions [6]. However, the effect of these distinctive hydrogen burning features at high strain rates on NOx emission for purely hydrogen lean laminar flames is still an open question. In this study counter-flow premixed hydrogen flames are investigated numerically to shed light on their behaviour under intensive level of strain, in particular the effect on NOx emissions.

Model and Setup

Detailed-chemistry one-dimensional and two-dimensional DNS analyses are performed for pure-hydrogen, lean, premixed, and strained laminar flamelets in a reactants-to-products counter-flow configuration. One-dimensional simulations are run with CHEM1D for a range of strain rate from $a = 100\ s^{-1}$ and $a = 10000\ s^{-1}$. Two-dimensional simulations are computed in OpenFOAM for only two representative high strain rates of $a = 2000\ s^{-1}$ and $a = 5000\ s^{-1}$. In both cases, detailed kinetic data of reactions from GRI3.0 mechanism are used, along with a mixture-averaged diffusion model. Lean conditions are established at an equivalence ratio of 0.7. The reactants temperature is fixed to 300K.

Results

The increase in burning rate with strain would suggest a corresponding increase of the flame temperature, thus NOx emissions. Counterintuitively, NOx emissions show a decreasing trend with strain in lean conditions, particularly at very high strain rates. In Fig. 1a, the NO flux form

1D and 2D (across the centreline) simulations is shown, demonstrating this decreasing trend. The NO flux is calculated as

$$\Phi_{NO,1D} = \int_x \rho Y_{NO} dx. \quad (1)$$

As shown in the right axis of Fig. 1a, the same trend is observed for the integral over the whole domain surface in the 2D simulations, suggesting that there is no additional NO formation across the flame-tangential direction.

Following the methodology of Ning et al. [2], the contribution of each NO pathway to the total NO formation has been reconstructed for two representative strain rates of $a = 2000\ s^{-1}$ and $a = 5000\ s^{-1}$. As reported in Fig. 1b, the analysis [2] shows that the main decrease of NO production with strain can be attributed to the thermal pathway. Nevertheless, this variation of NOx is not observed to be associated with a decrease of temperature [3], but rather on to the transport behaviour of the radicals involved in the formation reactions.

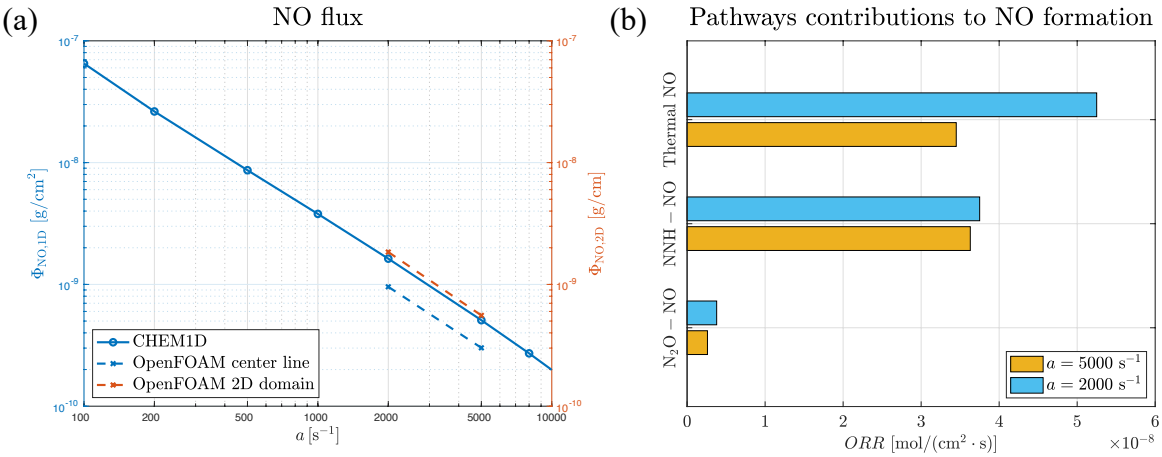

Figure 1. (a) Variation of NO flux with strain. (b) Contribution of each NO formation pathway to the total NO formation for two representative strain levels.

The focus is thus shifted on the OH radical, which was shown in the previous analysis to be involved in the main contributing reaction to the thermal NOx formation. A close inspection of the radical distribution across the flamelets (Fig.2) shows that the OH concentration as a higher peak at higher strain rates, but drops significantly downstream of the flame, thus suppressing the NO formation in the hot products.

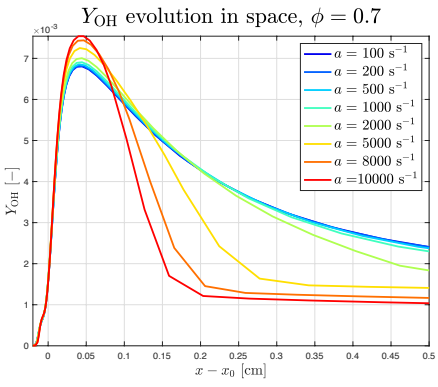

Figure 2. OH radical distribution

References

[1] Jackson et al., *Combustion and Flame* 132(3): 503–511 (2003).
[2] Ning et al., *International journal of hydrogen energy* 42(15): 10466–10474 (2017).
[3] Speth & Ghoniem, *Proceedings of the Combustion Institute* 32(2): 2993–3000 (2009).
[4] Liang et al., *Proceedings of the Combustion Institute* 36(1): 1137–1143 (2017).
[5] Vance et al., *Combustion and Flame* 237: 111729 (2022).
[6] Van Oijen et al., *Progress in Energy and Combustion Science* 57: 30–74 (2016).

INVESTIGATION OF SINGLE IRON PARTICLE COMBUSTION IN THE KNUDSEN TRANSITION REGIME

L.C. Thijs and X. Mi and J.A. van Oijen and L.P.H. de Goey
l.c.thijs@tue.nl
Department of Mechanical Engineering, Eindhoven University of Technology, Netherlands

Abstract

Metal fuels, powders of micron-sized metal particles are gaining attention as promising energy carriers [1]. Most of them have high energy densities, are inherently carbon free, recyclable and compact. Iron is considered as a promising metal fuel since it is widely available, cheap and has the possibility to burn heterogeneously, without the formation of nano-sized iron-oxide products [1, 2].

Understanding the burning process of a single iron particle is of key importance to be able to use iron as a metal fuel. In the numerical models for single iron particles [2–5], the continuum assumption is used to describe the reactive transport processes in iron particle combustion. In our previous work [2, 4], our model showed good agreement with experimental data when neglecting internal transport and assuming that the conversion of Fe to FeO is the relevant conversion up to the maximum temperature. However, in this work, only particles of 40 µm and 50 µm are investigated. If the size of the particle becomes too small (Knudsen number larger than 0.01), modelling the heat and mass transfer using the continuum approach becomes inaccurate.

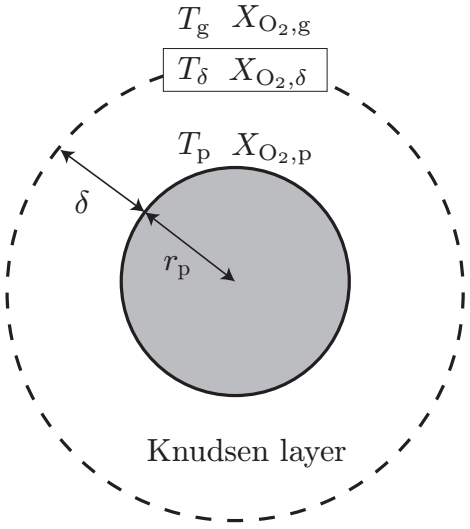

Figure 1. The configuration for heat and mass transfer analysis considered in the Knudsen model.

To model the mass and and heat flux in the Knudsen regime, a boundary sphere method is used [6]. Figure 1 illustrates the configuration which is used for the boundary sphere method. The particle is surrounded by a spherical Knudsen layer δ. Inside the Knudsen layer, the mass

and heat flux in the free-molecular regime are described, while outside the Knudsen layer the continuum approach is used.

To accurately describe the heat and mass transfer in the free-molecular regime, the thermal and mass accommodation coefficients should be known. The thermal accommodation coefficient (TAC) describes the average energy transfer when gas molecules scatter from the surface. The mass accommodation coefficient (MAC) or absorption coefficient is defined as the fraction of incoming oxygen molecules that upon collision with the iron surface are absorbed (accommodated) rather than reflected. Molecular dynamics simulations are often used to determine thermal [7] and mass accommodation coefficients [8]. However, none of them performed a systematic analysis on these coefficients for iron with air. Therefore, this work will use molecular dynamics simulations to determine the TAC and MAC. Subsequently, the obtained TAC and MAC values are used to investigate the effect of the Knudsen number of the combustion behavior of single iron particles.

References

[1] J. M. Bergthorson *et al.*, "Direct combustion of recyclable metal fuels for zero-carbon heat and power," *Appl. Energy*, vol. 160, pp. 368–382, 2015.

[2] L. C. Thijs, C. E. A. G van Gool, W. J. S Ramaekers, J. A. van Oijen, and L. P. H. de Goey, "Resolved simulations of single iron particle combustion and the release of nanoparticles," *Proc Combust Inst.*, 2023.

[3] T. Hazenberg and J. A. van Oijen, "Structures and burning velocities of flames in iron aerosols," *Proc Combust Inst.*, vol. 38, no. 3, pp. 4383–4390, 2021.

[4] L. C. Thijs, C. E. A. G van Gool, W. J. S. Ramaekers, J. G. M. Kuerten, J. A. van Oijen, and L. P. H. de Goey, "Improvement of heat- and mass transfer modeling for single iron particles combustion using resolved simulations," *Combust Sci Technol.*, vol. 0, no. 0, pp. 1–17, 2022.

[5] X. Mi, A. Fujinawa, and J. M. Bergthorson, "A quantitative analysis of the ignition characteristics of fine iron particles," *Combustion and Flame*, vol. 240, p. 112 011, 2022.

[6] F. Liu, K. J. Daun, D. R. Snelling, and G. J. Smallwood, "Heat conduction from a spherical nano-particle: Status of modeling heat conduction in laser-induced incandescence," *Appl. Phys. B*, vol. 83, 355–382, 2006.

[7] T. A. Sipkens and K. J. Daun, "Effect of surface interatomic potential on thermal accommodation coefficients derived from molecular dynamics," *J. Phys. Chem. C.*, vol. 122, no. 35, pp. 20 431–20 443, 2018.

[8] J. Nie, A. Chandra, Z. Liang, and P. Keblinski, "Mass accommodation at a high-velocity water liquid-vapor interface," *J. Chem. Phys.*, vol. 150, no. 15, p. 154 705, 2019.

METAL FUEL PRODUCTION: FLUIDIZED BED REDUCTION

C.J.M. Hessels, G. Finotello, Y. Tang, T.A.M. Homan, and N.G. Deen
c.j.m.hessels@tue.nl
Power and Flow group, Department of Mechanical Engineering, Eindhoven University of Technology
Eindhoven Institute for Renewable Energy Systems (EIRES), Eindhoven University of Technology

Abstract

Cyclic combustion and reduction of iron powder has become a promising dense carrier for renewable energy [1]. One option for the reduction process is to use a fluidized bed reactor, utilizing green hydrogen as reducing agent at operating temperatures around 800 K. In this work, the reduction behavior of combusted powder in a fluidized bed are presented. Subsequently, the differences between "regenerated" and "initial" iron powder are discussed.

The fluidized bed reactor used is presented in Figure 1. The powder used is the result of combustion of commercially available iron powder (Rio Tinto ATOMET 95) in a pilot scale industrial burner (combustion details are given in Choisez *et al.* [2]). The powder is subsequently sieved within the range of 32-100 μm in order to remove ultra-fines and large agglomerates. It removed around 15 wt% of the combusted powder.

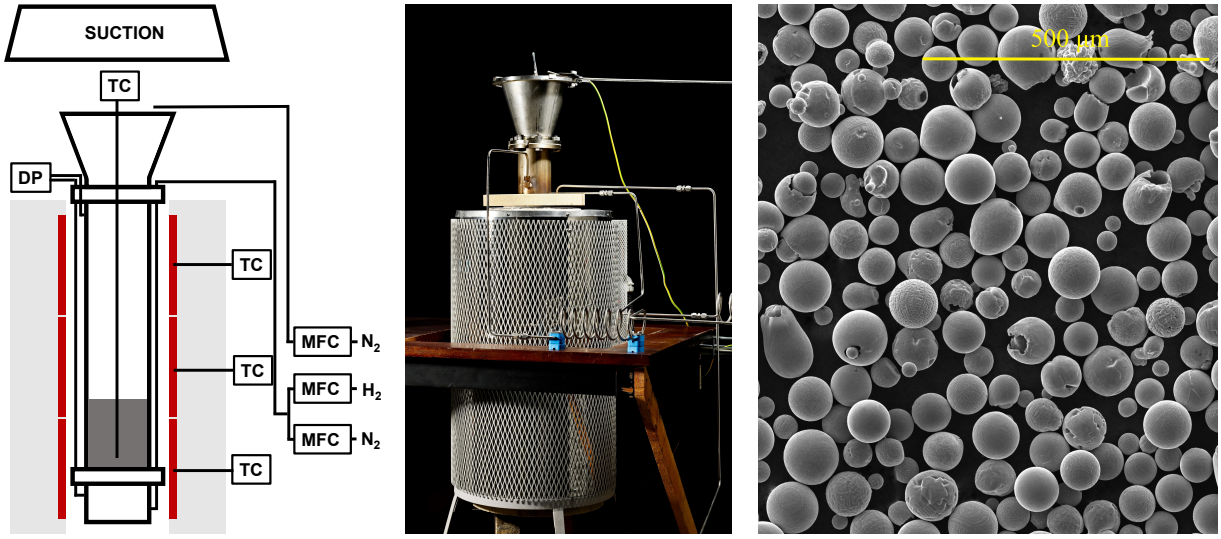

Figure 1. Left and center: schematic and photograph of the fluidized bed reactor, respectively. Right: SEM image of the combusted powder. Photograph courtesy of Bart van Overbeeke.

Reduction experiments are subsequently performed at various temperatures and hydrogen molar fractions. To keep the fluidization state constant, experiments are performed at constant excess velocity. More details on the fluidization behavior can be found in Hessels *et al.* [3]. A maximum reduction degree of 75.6% was obtained (after 9.5 hours) at 750 K with 100 vol% H_2.

The reduced (regenerated) powder is analyzed alongside the original (initial) powder from Rio Tinto for particle size, reduction degree and density. Scanning electron microscopy images of the powders are presented in Figure 2. The material properties are summarized in Table 1.

The results show that the initial powder is quite different from the combusted and regenerated powder in particle size and shape (smaller and less round, respectively). Furthermore, the reduced powder is roughly the same size as the combusted powder, but much more porous. This, in combination with a lower reduction degree, substantially lowers the energy density of the material in comparison with the initial powder.

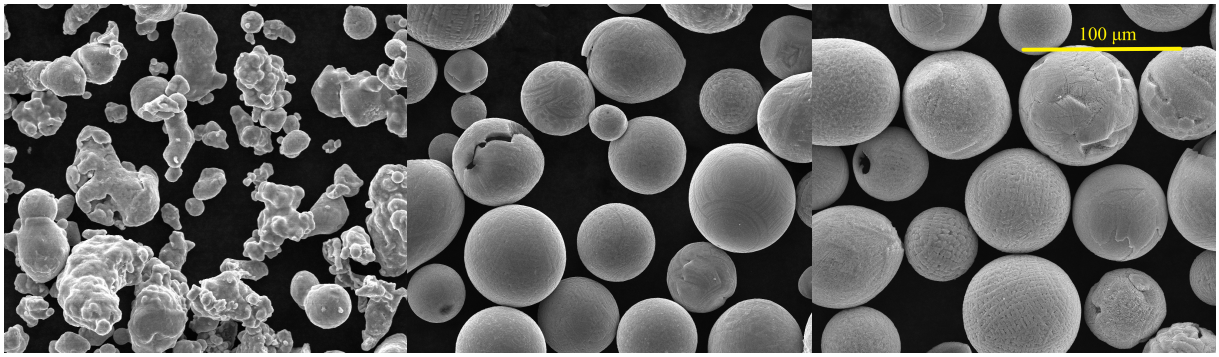

Figure 2. SEM images of: initial (left), combusted (center) and regenerated (right) iron power.

Table 1. Properties of initial, combusted and reduced powder.

Property	**Initial**	**Combusted**	**Regenerated**	**Unit**
Sauter diameter, d_{32}	29.2	52.1	52.9	µm
Average L/D, $\bar{LD}$	1.403	1.092	1.126	-
Bulk density[1], ρ_{b}	4027	2910	2320	kg/m^3
Particle density[2], ρ_{p}	7820	4700	3750	kg/m^3
Solid density, ρ_{s}	7820	5270	6835	kg/m^3
Internal porosity, ϵ_{p}	0	10	45	%
Reduction degree[3], RD	-	-	75.6	%
Ferrite content[4]	99	7	71	wt%
Energy density[5]	29.5	-	12.5	MJ/L
Specific energy	7.3	-	5.4	MJ/kg

[1] Measured using a 100 mL measuring cylinder containing the powder (vibrated).
[2] Based on a packing density of 0.62 (poured random packing) for the combusted and regenerated powder.
[3] Defined as the weight loss obtained during reduction, divided by the weight loss for full conversion to Fe.
[4] Defined as the weight of α-iron present, divided by the total mass.
[5] Based on the bulk density mentioned and combustion to Fe_2O_3.

References

[1] J. M. Bergthorson, S. Goroshin, M. J. Soo, P. Julien, J. Palecka, D. L. Frost, and D. J. Jarvis, "Direct combustion of recyclable metal fuels for zero-carbon heat and power," *Applied Energy*, vol. 160, pp. 368 –382, 2015.

[2] L. Choisez, N. E. van Rooij, C. J. M. Hessels, A. K. da Silva, I. R. Souza Filho, Y. Ma, P. de Goey, H. Springer, and D. Raabe, "Phase transformations and microstructure evolution during combustion of iron powder," *Acta Materialia*, vol. 239, p. 118 261, 2022.

[3] C. J. M. Hessels, D. W. J. Lelivelt, N. C. Stevens, Y. Tang, N. G. Deen, and G. Finotello, "Minimum fluidization velocity and reduction behavior of combusted iron powder in a fluidized bed," *Fuel*, vol. 330, p. xxxxxx, 2022 (under review).

IDENTIFICATION OF THERMOACOUSTIC BEHAVIOR OF MULTIPLE PERFORATION PATTERN VIA TRANSFER FUNCTION COMPOSITION APPROACH

Hamed F. Ganji[1*], Viktor Kornilov[1], Jeroen van Oijen[1], Ines Lopez Arteaga[1,2] and Philip de Goey[1]

[*] h.faghanpourganji@tue.nl

[1] Department of Mechanical Engineering, Eindhoven University of Technology, the Netherlands

[2]Department of Engineering Mechanics, KTH Royal Institute of Technology, Sweden

Abstract

An attractive approach to cope with the instability is the purposeful design of the burner thermoacoustics. For the particular case of premixed, burner deck anchored conical flames, the transfer function (TF) depends on the diameter of perforation. It suggests the concept of combining different size and shape of perforations in one burner deck. In the present work, the acoustic response of sintered ceramic fiber burners with mixed perforation is investigated using the TF (de)composition (TF(d)C) principle. By this approach, the cumulative flame TF can be represented as a weighted sum of elemental TF's of the groups of flames on the basis of the additive nature of the individual flame heat release rate. The capability of this principle to offer a designing framework for optimization of burner deck patterns aiming desirable acoustic characteristics will be tested by a course of measurements.

Introduction

The thermoacoustic instability arises from a closed-loop feedback between the unsteady combustion and the acoustic modes of the entire system[1]. An attractive approach to cope with the instability is the purposeful design of the burner thermoacoustics[2]. There is a heuristic idea that the acoustic response of one flame type can be compensated or cancelled by other flame types[2, 3]. In the current work, we focus on this idea to investigate the possibility of such flame TF superposition for composite burners.

Methodology

A common practice to quantify the interaction of the flame with acoustic waves in the frequency domain is by the so-called flame TF, which is defined as the ratio of the relative heat release rate perturbation ($\hat{Q}'/\bar{Q}$) and the relative flow perturbation ($\hat{v}'/\bar{v}$)

$$F(\omega) = \frac{\hat{Q}'}{\hat{v}'}\frac{\bar{v}}{\bar{Q}} \tag{1}$$

In the general case of a composite burner deck, when the type of deck structure and flame pattern are not specified, the concept of flame TF composition can be mathematically formulated as follows:

$$F_\Sigma(\omega) = \sum_{k=1}^{n_k} F_k(\omega)\Omega_k, \qquad \Omega_k = \frac{N_k A_k \bar{v}_k}{A_B \bar{v}} \tag{2}$$

where F_Σ is the composite TF and N_k, A_k and $\bar{v}_k$ are the number of flames in group k, open area corresponding to an individual perforation in group k and velocity of the combustible flow that goes through the perforations in group k, respectively. A_B and $\bar{v}$ indicate the total area of the burner and inflow upstream velocity. In practice, N_k, A_k, A_B and $\bar{v}$ are given, so to determine the TF of the composite burner deck, the remaining task is to obtain knowledge of the local mean flow $\bar{v}_k$ and the TF of the segmental flames $F_k(\omega)$. One straightforward approach could be to perform the pressure

drop (PD) measurement. It enables us to find the operating conditions for measuring the flame TF of a burner with uniform perforation to (de)compose the TF. In the current work, we determine the flame TF of basic burners with uniform perforations experimentally[2].

Results discussion

In this work, we use a specific ceramic burner, which exhibits the flame TF gain quite higher than usual in some operating condition. We leave the discussion about this observation for the future work. The black solid curve in Figure 1 represents the flame/burner TF for mixed perforation burner based on elemental/uniform burners (the blue and red curves). To prove the concept of TF(d)c, a direct TF measurement is performed on this composite sample, which is indicated with black dashed color in the figure. The comparison with the model-based TF (black solid curve) shows a qualitatively and quantitatively satisfactory agreement both in the gain and in the phase of the cumulative TF.

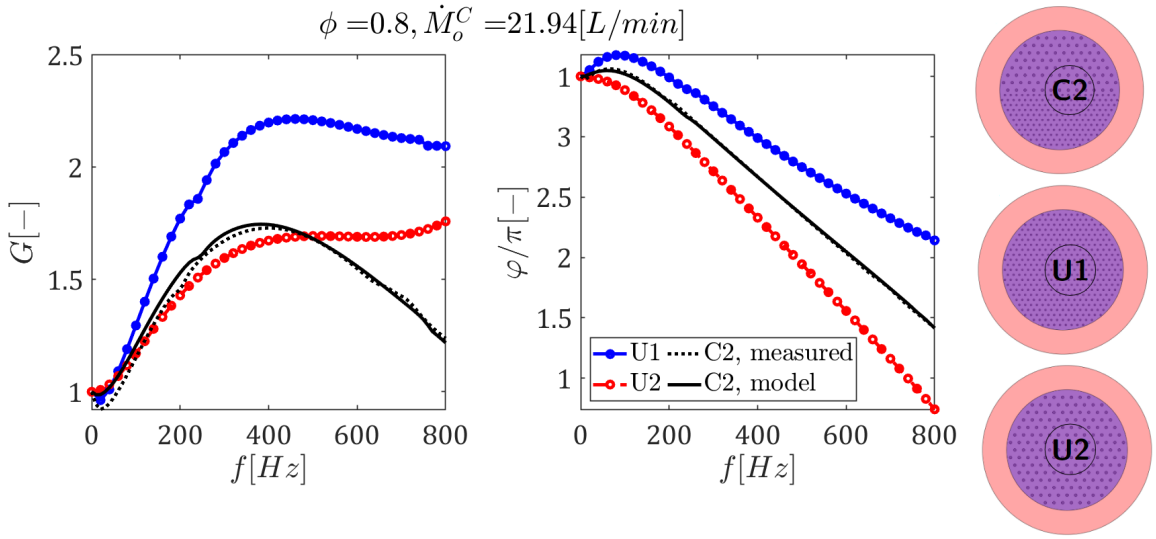

Figure 1. Comparison of measured and predicted flame TF. gain (right) and phase (left) for partitioned composite burner deck at medium thermal power.

Conclusion

The principle of flame transfer function (de)composition from individual components has been experimentally demonstrated for generic burner deck patterns that are relatively porous. This study demonstrated the efficiency and validity of the TF(d)c principle as a tool for burner stabilization. In addition, Two configurations have been considered to provide an intuitive picture of the limitation and validity of this principle: i) a mixed perforation burner deck, ii) a partitioned perforation burner deck. In addition, results obtained from TF(d)c principle showed better predictability for partitioned composite burners rather than the mixed perforation burners in the full thermal power range.

Reference

[1] M Hoeijmakers, "Flame-acoustic coupling in combustion instabilities [phd thesis]," *The Netherland: Technische Universiteit Eindhoven*, 2014.

[2] V. Kornilov, M Manohar, and L. de Goey, "Thermo-acoustic behaviour of multiple flame burner decks: Transfer function (de) composition," *Proceedings of the Combustion Institute*, vol. 32, no. 1, pp. 1383–1390, 2009.

[3] S Kagiya, "New burner design technique for suppression of combustion oscillations, tokyo-gas co.," *Energy and Environmental Technology Laborator*, 2000.

Direct measurements of preferential diffusion in turbulent H_2 flames using multi-field CARS imaging

Leonardo Castellanos* Francesco Mazza* and Alexis Bohlin **
L.J.CastellanosGonzales@tudelft.nl
*Faculty of Aerospace Engineering, Delft University of Technology, the Netherlands
**Faculty of Computer Science, Electrical and Space Engineering, Luleå University of Technology, Sweden

Abstract

Hydrogen (H_2) is a promising energy carrier for the advancement of future carbon-free combustion technologies. In this scenario, the direct measurement of the entire set of scalars involved in the combustion process of H_2 is required to fully understand its flame propagation mechanism. The coupling of simultaneously measured temperature and local concentration of species allows the investigation of molecular interdiffusion processes affecting the structure of these flames. For instance, information about the preferential transport of H_2 caused by differences between molecular diffusion coefficients of the reactants, and products, can be used for the development and improvement of combustion models in which it is normally assumed that atomic mass fractions are conserved from reactants to fully burnt products [1].

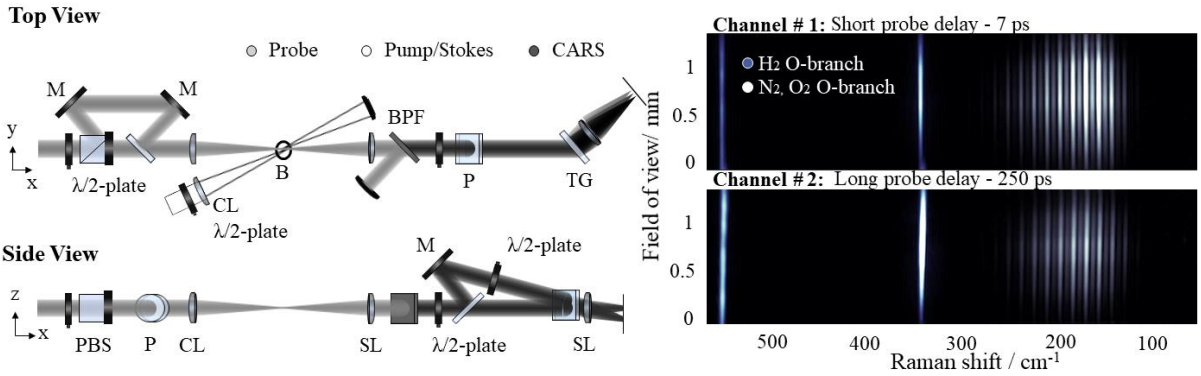

Figure 1. Experimental set-up developed to perform spatiotemporal CARS. A short delay probe is used to measure temperature as well as H_2 and O_2 concentration. The long delay probe is employed to deduce water vapor concentration based on the dephasing of the pure-rotational N_2 CARS signal. Both signals are acquired simultaneously using a polarization sensitive coherent imaging spectrometer.

In this work, we developed a one-dimensional (1-D) coherent anti-Stokes Raman scattering (CARS) instrument for simultaneous single-shot imaging of temperature and major species concentration in H_2/air flames. A single regenerative amplifier system (Astrella, Coherent) combined with a second-harmonic bandwidth compressor (SHBC, Light conversion) provides auto-synchronized pump/Stokes (35 fs full-width-at-half-maximum, FWHM) and probe (13 ps FWHM) electromagnetic fields which are intersected in a crossed plane geometry forming a one-dimensional field of view (Fig. 1). The pure-rotational CARS spectra from nitrogen, oxygen, and hydrogen are generated at a short pump/Stokes-probe delay, therefore, minimizing the influence of collisions on the signal. A second picosecond-ps pulse generated using a polarization separation method probes the coherence induced by the pump/Stokes photons 250

ps later, and the generated CARS signal is used to deduce the H_2O vapor concentration based on the dephasing rate of the N_2 CARS signal caused by inelastic collisions with H_2O. The two signals generated using this collinear dual-probe approach are detected simultaneously in two distinct detection channels of our unique polarization-sensitive coherent imaging spectrometer

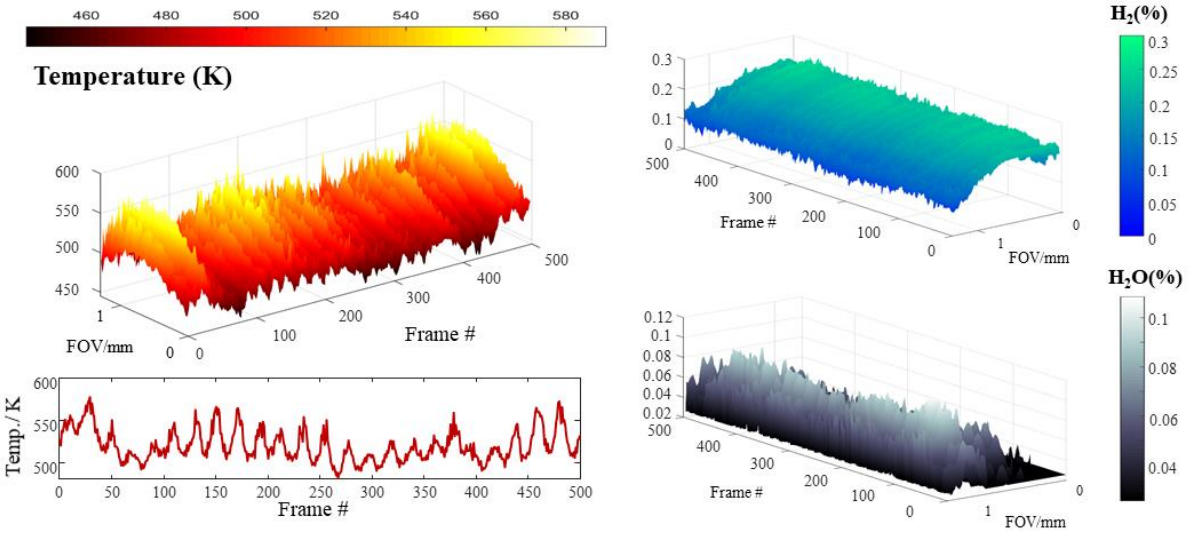

using an acquisition rate of 250 Hz [2].

Figure 2. Cinematographic 1D-CARS thermometry and species concentration acquisition across 1.4 mm field of view. The probe volume is located in the fuel stream of the H_2-N_2 diffusion flame 4 mm above the nozzle.

The developed CARS instrument is tested in the turbulent TU Darmstadt/DLR Stuttgart canonical 'H3 flame'. The burner consists of a straight stainless steel tube, with 8 mm inner diameter (D), that provides a 1:1 mixture (in volume) of N_2-H_2 flow. A concentric contoured nozzle, with an inner diameter of 140 mm, provides a coflow of dry air. Measurements were performed at three different heights above the burner rim: x/D= 0.5, 2.5 and 5. Figure 2, presents the simultaneous temperature, H_2 and H_2O concentration evolution in time 1.4 mm snapshots in the fuel stream. The correlated space-time resolution of the instrument prove sufficient for tracking the position of the flame during the entire acquisition time. To the best of our knowledge, this is the first time that the entire scalar field of a H_2/air flame is simultaneously acquired using CARS spectroscopy. The data obtained from these measurements will be used to study the preferential transport of H_2 molecule and its effect on the local flame structure.

Acknowledgements

We gratefully acknowledge the financial support provided by the Netherlands Organization for Scientific Research (NWO), obtained through a Vidi grant in the Applied and Engineering Sciences domain (AES) (15690). In addition, A. Bohlin is thankful for support through the RIT (Space for Innovation and Growth) project/European Regional Development Fond in Norrbotten, Sweden.

[1] Barlow, R. S., Dunn, M. J., Sweeney, M. S., & Hochgreb, S., "Effects of preferential transport in turbulent bluff-body-stabilized lean premixed CH4/air flames". *Comb. and Flame* 256:2575 (2012)

[2] Mazza, F., Castellanos, L., Kliukin, D., & Bohlin, A., "Coherent Raman imaging thermometry with in-situ referencing of the impulsive excitation efficiency". *Proc. Comb. Inst*. 1895:1904 (2021),.

Ultrabroadband coherent Raman spectroscopy for methane thermometry and relative concentration measurements

Francesco Mazza[1], Ona Thornquist[1], Leonardo Castellanos[1], Thomas Butterworth[2] and Alexis Bohlin[1,3]

f.mazza@tudelft.nl

[1]Advanced Laser Diagnostics and Flames Laboratory, Delft University of Technology, Kluyverweg 1, 2629 HS Delft, The Netherlands

[2]Faculty of Science and Engineering, Maastricht University, Paul Henri Spaaklaan 1, 6229 GS Maastricht, The Netherlands

[3]Space Propulsion Laboratory, Luleå University of Technology, Bengt Hultqvists väg 1, 981 92 Kiruna, Sweden

Abstract

Methane (CH_4), the simplest hydrocarbon molecule, plays an important role anthropogenic climate change as well as in novel energy conversion technologies [1]. In particular, CH_4 pyrolysis has been proposed for the carbon-neutral production of hydrogen (H_2), with residual carbon in non-oxidised solid form [2]. Understanding the CH_4 chemistry via *in-situ* measurements in chemically-reacting environments is thus critical to its commercial utilisation to produce commodity chemicals [3]. CH_4 has been the subject of several spectroscopic studies based e.g. on infrared laser absorption and spontaneous Raman scattering. These linear techniques can suffer from limited signal strength in harsh, luminous environments and, in the case of absorption spectroscopy, limited spatial resolution: Femtosecond/picosecond (fs/ps) coherent Raman spectroscopy (CRS) could greatly benefit the investigation of CH_4 chemistry, providing high-resolution *in-situ* measurements.

Fs/ps CRS has been recently applied on the vibrational ν_1 mode of CH_4 at ~2900 cm^{-1}, in the so-called "Pentad" region [4]. The "Dyad" region of the CH_4 spectrum (~1000-2000 cm^{-1}), due to the vibrational bending of the H-C-H bonds (ν_2 mode) has often been overlooked, owing to the lower scattering cross-section associated this vibrational mode. The application of ultrabroadband fs/ps CRS on the CH_4 ν_2 spectrum offers the possibility of multi-species detection as the ro-vibrational spectra of oxygen (O_2) and carbon dioxide (CO_2) also appear in this region [5], as does the pure-rotational spectrum of H_2. In the present work, we demonstrate single-shot detection of the ro-vibrational ν_2 mode spectrum of CH_4 at high temperature across a laminar CH_4/air diffusion flame, as well as of the CO_2, O_2 and H_2 spectra, as shown in Fig. 1.

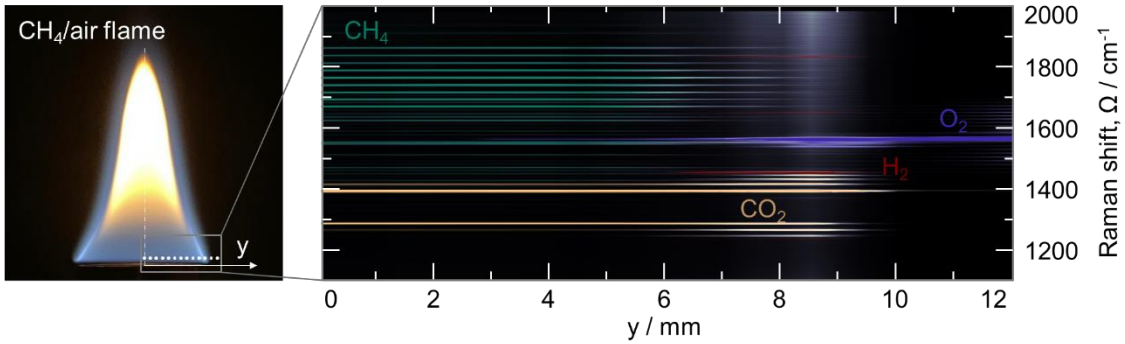

Figure 1. Spatially-resolved ultrabroadband fs/ps CRS performed across a laminar CH_4/air diffusion flame front. The ro-vibrational spectra of CO_2, O_2, CH_4, and the pure-rotational spectrum of H_2 are acquired in the region 1200-2000 cm^{-1}. Note that gamma compression is applied to the image to highlight some of the spectral features.

Spatially resolved measurements allow for monitoring the physical-chemical processes in this environment, in particular the pyrolysis of CH_4 and production of H_2 in the reaction layer of the flame. A time-domain model of the CH_4 ν_2 CRS spectrum, including over 10 million spectral lines, is used to extract temperature information from the CH_4 CRS signal, and CH_4 CRS thermometry is validated against CO_2 CRS [5], with an accuracy better than 3% at all measurement locations (Fig. 2).

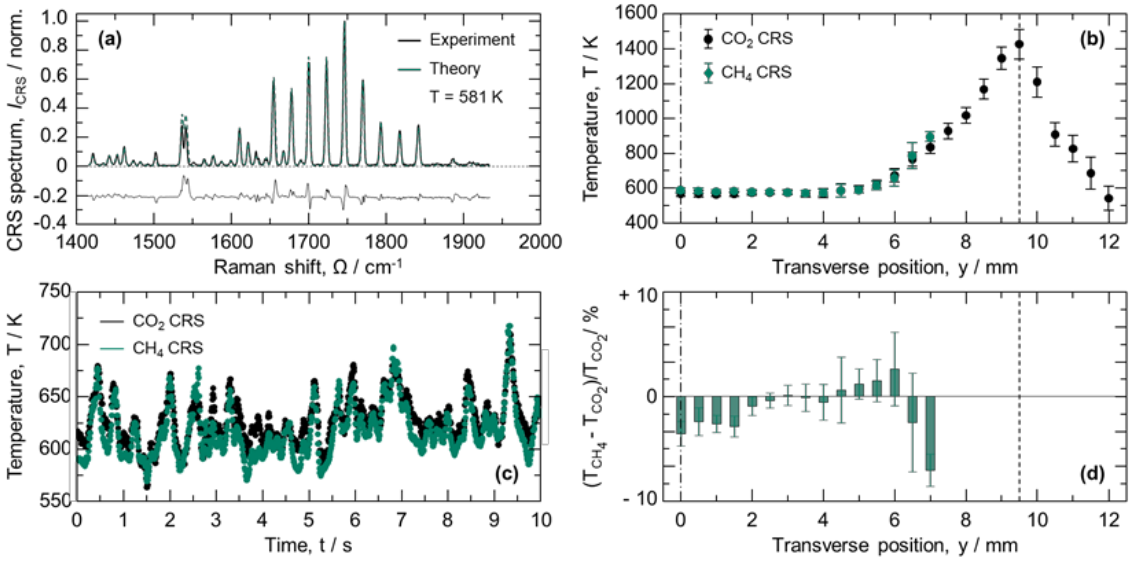

Figure 2. Ro-vibrational CH_4 ν_2 CRS thermometry across a laminar CH_4/air diffusion flame front. (a) Experimental 10-shot-averaged CH_4 ν_2 CRS spectrum and comparison to time-domain model. (b) Validation of the CH_4 ν_2 CRS thermometry by ro-vibrational CO_2 CRS thermometry. (c) Temperature fluctuations over 10 s at location y=5.5 mm, measured by CH_4 ν_2 and CO_2 CRS. (d) The accuracy of the CH_4 ν_2 CRS thermometry, validated against CO_2 CRS, is better than 3% at all measurement locations.

Acknowledgements

We gratefully acknowledge the financial support provided by the Netherlands Organization for Scientific Research (NWO), obtained through a Vidi grant in the Applied and Engineering Sciences domain (AES) (15690). A. Bohlin is thankful for support through the RIT (Space for Innovation and Growth) project/European Regional Development Fund in Kiruna.

References

[1] Y.A. Ba, C. Wenger, R. Surleau, V. Boudon, M. Rotger, L. Daumont, D.A. Bonhommeau, V.G. Tyuterev, and M.L. Dubernet, "MeCaSDa and ECaSDa: Methane and ethene calculated spectroscopic databases for the virtual atomic and molecular data centre", *J. Quant. Spectrosc. Radiat. Transf.* 130**:** 62-68 (2013).

[2] *Hydrogen strategy: enabling a low-carbon economy*, U.S. Department of Energy, Washington D.C.

[3] T. Butterworth, A. van de Steeg, D. van den Bekerom, T. Minea, T. Righart, Q. Ong, and G. van Rooij, "Plasma induced vibrational excitation of CH_4–A window to its mode selective processing" *Plasma Sources Sci. Technol.* 29, 095007 (2020).

[4] T.Y. Chen, C.J. Kliewer, B.M. Goldberg, E. Kolemen, and Y. Ju, "Time-domain modelling and thermometry of the CH_4 ν_1 Q-branch using hybrid femtosecond-picosecond coherent anti-Stokes Raman scattering", *Comb. Flame*, 224:183-195 (2021).

[5] F. Mazza, N. Griffioen, L. Castellanos, D. Kliukin, and A. Bohlin, "High-temperature rotational-vibrational O_2-CO_2 coherent Raman spectroscopy with ultrabroadband femtosecond laser excitation generated *in-situ*", *Comb. Flame*, 237:111738 (2022).

FLOW FIELD ANALYSIS OF A SWIRL STABILIZED PREMIXED HYDROGEN COMBUSTOR WITH AXIAL AIR INJECTION AT NON-REACTING CONDITIONS

K. Dave, S. Vermeijlen, R. Sampat and A. Gangoli Rao
K.A.Dave@tudelft.nl
Sustainable Aircraft Propulsion, Flow Physics and Technology Department,
Faculty of Aerospace Engineering, Delft University of Technology.
Kluyverweg 1, 2629 HS Delft, Netherlands.

Abstract

Hydrogen as a carbon-neutral energy carrier is an attractive alternative to hydrocarbon fuels for powering future aircraft engines. However, NO_x emissions still arise with hydrogen-air combustion and therefore will have to be addressed. Lean premixed combustion is one of the methods to achieve low NO_x emissions, but premixed hydrogen systems have a high tendency for flashback due to high flame speeds for hydrogen-air mixtures. The current research aims to develop a lean premixed swirl-stabilized hydrogen combustor for future aero-engine applications. It has been shown that a non-swirling axial jet of air can be applied at the centerline to enhance the resistance to core flashback [1]. This paper reports the findings of experiments performed to build and expand upon this concept and gain more insights into the use of axial air injection (AAI) while designing a lean premixed swirl-stabilized hydrogen combustor.

The main objectives of this study include understanding the effect of swirler type, swirl number and varying amounts of AAI on an isothermal, non-reacting flow field of a premixed swirl-stabilized combustor. A comparison of the performance of several radial and axial swirlers in controlling/manipulating the combustor flow field by varying the AAI fraction under isothermal, non-reacting conditions is present. Geometric swirl numbers ranging from 0.7 – 1.5 and AAI fractions ranging from 0 – 40% were investigated.

PIV measurements made in the center and cross planes were used to visualize the velocity fields in the mixing tube and the combustor. An effective swirl number near the outlet of the mixing tube was calculated using these velocity fields. It was observed that the effective swirl number decreases with an increasing amount of AAI. This is thought to be due to two reasons. Firstly, an increase in AAI causes the mass flow through the swirler to be diverted and injected through the AAI port. The redistribution of mass flow changes the velocity distribution such that the initial swirl number at the mixing tube inlet itself is reduced. Secondly, a non-swirling AAI jet introduces an additional shear layer in the center of the swirling jet that enhances the degradation of the tangential velocity component in the mixing tube. The effect of shear layer interaction is expected to increase with increasing AAI fraction resulting in greater degradation of swirl number in the mixing tube. The relative strength of these two effects will be analyzed in a future study. The effect of fuel addition was also found to be the same and the effective swirl number at the mixing tube outlet decreased with increasing equivalence ratio. Although the mechanisms by which this occurs were found to be different in the case of radial and axial swirlers. For radial swirlers with axially oriented fuel injection, the fuel jets affect the flow field in the same way as AAI, albeit to a lesser extent because of the lower flow rates. In case of axial swirlers, the radially oriented fuel jets impinge on the swirling jet and reduce the effective swirl number. This effect is expected to increases with an increasing equivalence ratio.

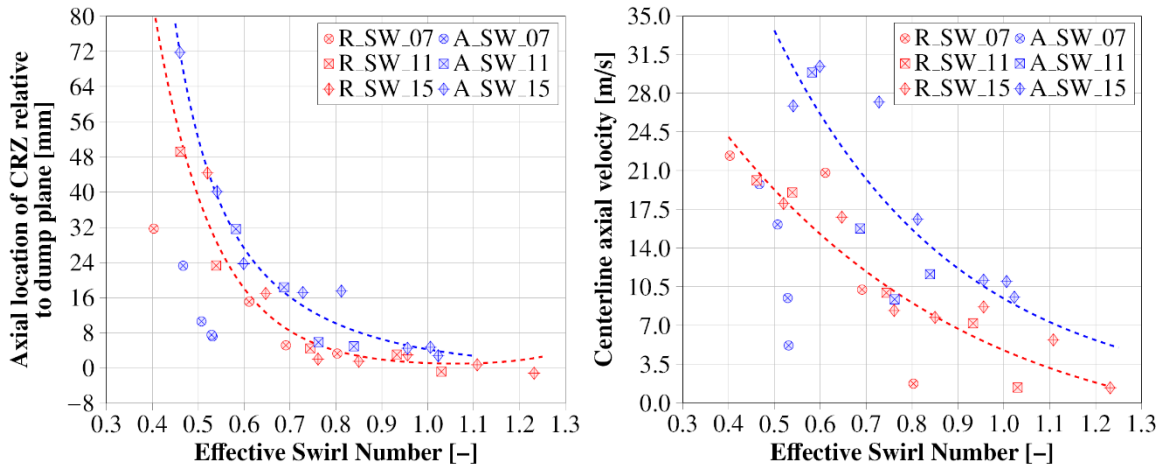

(a) (b)

Figure 1 Variation of (a) location of CRZ & (b) centerline axial velocity at mixing tube outlet with effective swirl number

From a phenomenological perspective, AAI changes the flow field in the combustor by reducing the effective swirl number at the end of the mixing tube and increasing the axial velocity component on the centerline of the swirling jet. This has been shown in a reduced form by plotting the location of the Central Re-circulation Zone (CRZ) and centerline axial velocity component as a function of the effective swirl number at the outlet of the mixing tube in figure 1. Both, the location of CRZ and centerline axial velocity were seen to vary exponentially with effective swirl number. In most cases, axial swirlers were found to have a more downstream location of CRZ and a higher centerline axial velocity at the mixing tube outlet for any given effective swirl number. Therefore, they are considered more favorable from the point of view of increasing core flashback resistance.

It was seen that an increase in AAI influences the velocity distribution inside the mixing tube which results in a reduction of the effective swirl number at the end of the mixing tube. A lower effective swirl number pushes the CRZ downstream while showing higher velocities along the centerline, both of which may assist in core flashback prevention. However, there is a possibility that the re-circulation reduces with reducing effective swirl numbers [2] and this opposes the principle of flame stabilization in swirl burners. Thus, the problem is reduced to one where CRZ location and velocity are a function of the effective swirl number at mixing tube outlet which can be manipulated using AAI to achieve an optimal operating condition for flame stabilization as well as flashback prevention. To maximize the desirable effects of AAI, a careful selection of a combination of several design parameters discussed in this paper may be required. Taking both the desirable and undesirable impacts into account, the results suggest that axial swirlers with inherently higher centerline velocities tend to have an advantage (over radial swirlers) as they would require lower AAI fractions in general to achieve similar centerline velocities and effective swirl numbers at the outlet of the mixing tube.

References

[1] Reichel, T. G., Terhaar, S., & Paschereit, O. (2015). Increasing flashback resistance in lean premixed swirl-stabilized hydrogen combustion by axial air injection. *Journal of Engineering for Gas Turbines and Power*, *137*(7), 071503.

[2] Weber, R., & Dugué, J. (1992). Combustion accelerated swirling flows in high confinements. *Progress in Energy and Combustion Science*, *18*(4), 349-367.

TOWARDS PLASMA-ASSISTED IGNITION-STABILIZED LEAN COMBUSTION

Ravi Patel*, Jeroen van Oijen*, Sander Nijdam and Nico Dam***
r.b.patel@tue.nl
*Department of Applied Physics, Eindhoven University of Technology, the Netherlands
**Department of Mechanical Engineering, Eindhoven University of Technology, the Netherlands

Abstract

Due to the increased risk of global warming, more and more emphasis is given on making combustion systems efficient and clean. Many combustion problems can be solved by operating combustion at low temperatures, i.e. in lean conditions. Unfortunately, ignition and flame stabilization become more and more difficult as we go towards the lean flammability limit. In recent years, the combustion community is empathizing on auto-ignition driven conditions that can stabilize combustion with lower heat release. Auto-ignition is achieved either by preheating the unburnt mixture or mixing it with fully or partially burnt exhaust products, i.e. in MILD combustion [1]. Plasma, being an efficient and fast source of radicals and heat, can be a useful tool to support the ignition in extreme conditions and hence ignition stabilized combustion [2]. One of the most popular examples of plasma-assisted combustion (PAC) is a spark plug. A spark is a thermal equilibrium plasma that heats up the fuel-air mixture locally. However, non-equilibrium plasmas are another class of plasmas which have a much higher electron temperature than gas temperature. High energy electrons are very efficient in producing a pool of radicals through various non-equilibrium pathways [2].

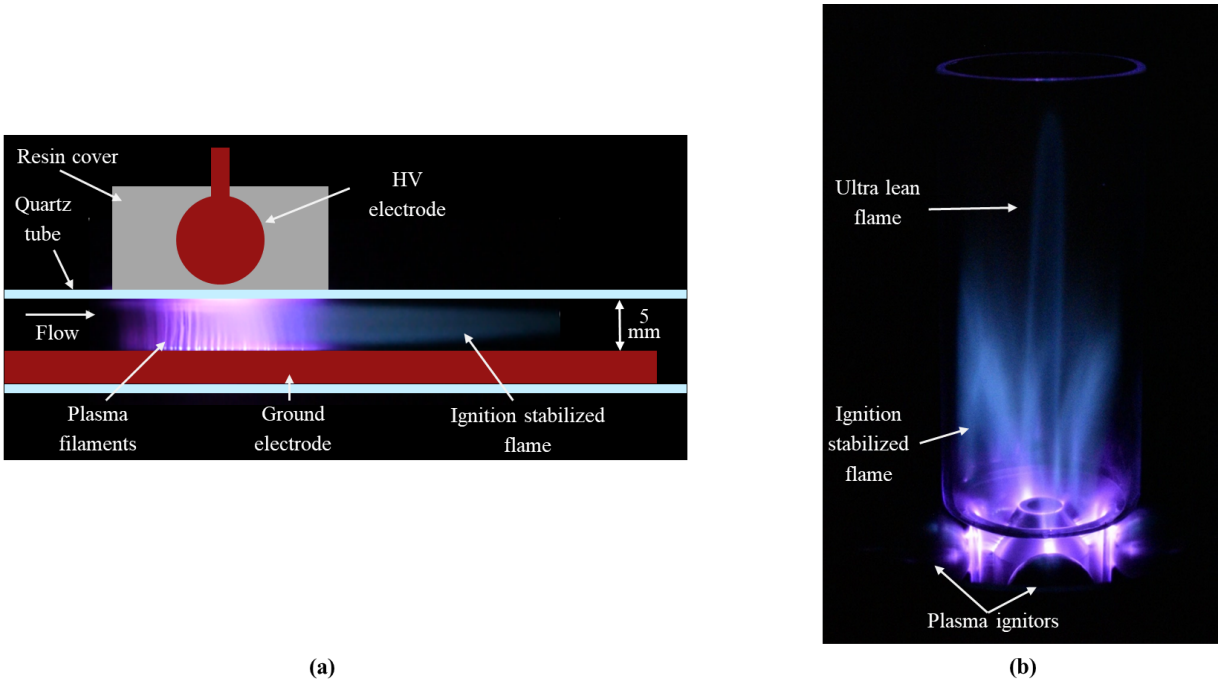

Figure 1. Digital camera photographs capturing ignition stabilized combustion in (a) a quartz flow channel reactor (b) a coaxial multi-channels burner.

In this work, experimental studies on dielectric barrier discharge (DBD) plasma-assisted ignition in methane-air flows have been performed in two configurations. The schematic and digital camera photograph of the first reactor used is shown in Figure 1 (a). It is a flow tube DBD configuration with a 5 mm discharge gap. DBD configuration has a ball-shaped high voltage electrode which is embedded inside the resin. The embedded high electrode is placed on top of the quartz tube and the ground electrode is placed inside the tube. The discharges are produced by 10 ns duration high voltage pulses at a maximum of 3 kHz PRR (Pulse Repetition Rate). The image is taken using a Nikon D5600 camera with 1/30 s exposure at 700 mbar pressure, 100 cm/s flow speed, 0.6 equivalence ratio of a methane-air mixture, and 2 kHz PRR. An elongated flame is visible outside the plasma region in the downstream direction. This stable-looking flame is a time-averaged image of repetitively ignited kernels. To examine this phenomenon better, high-speed intensified imaging is performed for various parameters along with phased-locked optical emission spectroscopy.

The first configuration enabled us to study the plasma-assisted ignition dynamics of a single ignition train. A second configuration has been developed to study the interaction between multiple ignition trains. Furthermore, the two flow channels configuration allows to explore the repetitively ignited kernel interaction with the virgin stream of the fuel-air mixture. In Figure 1 (b), a digital camera photograph of the reactor in operation is shown. Flow speeds and equivalence ratios in the outer and inner channels are 0.55 and 150 cm/s, and 0.35 and 150 cm/s respectively. It is important to note that the flame blows out at this condition without plasma support. In the photograph, two flame fronts are visible. The outer front is stabilized by plasma-assisted repetitive ignition and the inner front by the interaction between hot ignition kernels and the methane-air flow below the lean flammability limit. Further analysis is required to gain more insight into the dynamics and combustion efficiency.

Acknowledgements
This work is part of the research programme "Making plasma assisted combustion efficient" with project number 16480, which is partly financed by the Dutch Research Council (NWO).

References

[1] A. Cavaliere and M. de Joannon, "Mild combustion," *Progress in Energy and Combustion science*, vol. 30, no. 4, pp. 329–366, 2004.

[2] Y. Ju and W. Sun, "Plasma assisted combustion: Dynamics and chemistry," *Progress in Energy and Combustion Science*, vol. 48, pp. 21–83, 2015.

INCLUSION OF DIFFERENTIAL DIFFUSION MODELS IN FLAMELET-PRESUMED PDF LES OF A LIFTED H_2 FLAME IN VITIATED COFLOW

G. Ferrante[1,*], **B. Kruljevic**[1], **I. Langella**[1]
g.ferrante@tudelft.nl
[1]Faculty of Aerospace Engineering, Delft University of Technology,
2629 HS Delft, The Netherlands

Introduction

The development of hydrogen lean burn technologies in aviation is attractive due to carbon-free combustion, high energy density and the possibility to control nitric oxides (NO_X) formation associated with the high flame temperature. In lean premixed flames, the faster diffusion of hydrogen towards the flame front with respect to the other species (differential diffusion DD) causes local variations of equivalence ratio and redistribution of enthalpy, which can ultimately lead to thermo-diffusive instabilities and cellular burning structures.

In the present study, strategies to implement DD models for turbulent combustion in flamelet based LES (large eddy simulation) with presumed probability density function (PDF) closure are explored. First, non-unitary Lewis number ($Le \neq 1$) diffusion transport is adopted at the tabulated thermo-chemistry level, only including effects of DD on the reaction rate. Subsequently, effects on the mixture fraction distribution at the resolved level are taken into account by adopting the method proposed by Regele et al. [1].This model, derived for laminar premixed flames, was proven to correctly capture 2D thermo-diffusive instabilities due to mixture fraction redistribution, and is extended here to account for the effect of turbulence consistently with the presumed PDF approach. Simulations are performed in this study with different DD inclusion approaches and results are compared with measurements available in the literature.

Case and Methodology

A LES model based on unstrained premixed flamelets with presumed PDF closure [2], is employed to simulate the turbulent lifted hydrogen flame in vitiated coflow studied by Cabra et al. [3]. The strong flame sensitivity to the fuel-oxydiser mixing, affected by differential diffusion, makes it a suitable test case for the investigation of DD effects and its modelling. The Favre-filtered Navier Stokes equations including conservation of mass, momentum and absolute enthalpy (sum of sensible and formation enthalpies) are solved along with four controlling variable to account for the turbulent-chemistry interaction. The sub-grid scale (SGS) stresses in the filtered momentum equation are closed using a one-equation model as in [2].

The simulated cases are reported in Table 1. In Case A no differential diffusion model is adopted. In cases C and D $Le \neq 1$ is assumed in the flamelet database. In cases B and D a filtered source term $\widetilde{\dot{\omega}_z}$ built on the progress variable gradient at the flamelet level is included in the mixture fraction transport equation [1]. This would allow to describe the mixture fraction redistribution at a resolved level.

Table 1: Simulated cases, inclusion of differential diffusion (DD) in the tabulated chemistry and at resolved scales in LES.

	Case A	Case B	Case C	Case D
Flamelets	$Le = 1$	$Le = 1$	$Le \neq 1$	$Le \neq 1$
LES	no DD	$\int_0^1 \int_0^1 \dot{\omega}_z(c,z)P(c,z)dc\,dz$	no DD	$\int_0^1 \int_0^1 \dot{\omega}_z(c,z)P(c,z)dc\,dz$

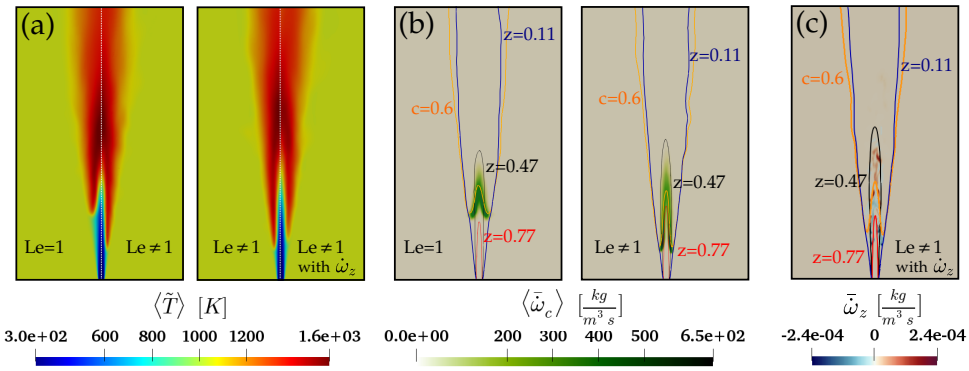

Figure 1: Mid-plane contours of: a) mean temperature , b) mean reaction rate, c) instantaneous mixture fraction source term. Isolines for stoichiometric, lean and rich limit are marked in black, blue and red respectively. The isoline for $\widetilde{c} = 0.6$ is marked in orange.

Results

A satisfactory agreement of the predicted average temperature and mixture fraction fields and their rms with experimental measurements is obtained for all the four cases. All models predict a lifted flame, stabilising between 7D and 12D and extending up to 26 D, in agreement with experiments. From the contour plot of the average reaction rate in Fig. 1b, a small region stabilising at lean conditions at the flame base and a long rich reacting layer in the central core can be observed. A major effect of the diffusion transport model used in the flamelet database calculation was observed. In addition to an overall reduction of the reaction rate peak, the inclusion of differential diffusion at thermochemistry level causes an increase of the reaction rate in the rich-stabilizing inner core and a decrease in the lean region, causing an upstream shift of the flame base $\sim 7D$ as compared to cases A and B $\sim 12D$). No relevant differences are observed between cases A and B, i.e. when DD is only modelled as mixture fraction redistribution at a resolved level. However some effect is observed when the DD is also taken into account at the flamelets level (cases C and D). Figure 1c shows the intensity and topology of $\widetilde{\dot{\omega}_z}$ in the LES domain when the $Le \neq 1$ diffusion model is employed in the flamelets. The gradients of progress variable, identifiable with the regions of temperature increase, lead to negative values of $\widetilde{\dot{\omega}_z}$ on the unburnt side in proximity of the flame front and to positive values on the burnt side. This is in line with what observed by Regele et al. [1] for the laminar case and describes the fast diffusion of hydrogen towards the flame front. The effect of mixture fraction redistribution is only dominant in the inner region of the flame brush, close to the flame anchoring point. In general, the modelling of $\widetilde{\dot{\omega}_z}$ produces a slight shift of the flame base downstream, and leads to a shorter flame, which better compares with the measurements. This is in turn caused by the decrease of reaction rate in the lean region at the flame base and the higher reaction rate in the richer inner region downstream.

References

[1] Regele, J.D., Knudsen, E., Pitsch, H., Blanquart, G., "A two-equation model for non-unity Lewis number differential diffusion in lean premixed laminar flames", *Combust. Flame* 160(2): 240–250 (2013).

[2] Chen, Z.X., Langella, I., Swaminathan, N., Stöhr, M., Meier, W., Kolla, H., "Large Eddy Simulation of a dual swirl gas turbine combustor: Flame/flow structures and stabilisation under thermoacoustically stable and unstable conditions", *Combust. Flame* 203: 279–300 (2019).

[3] Cabra, R., Myhrvold, T., Chen, J.Y., Dibble, R.W., Karpetis, A.N., Barlow, R.S., "Simultaneous laser Raman-Rayleigh-LIF measurements and numerical modeling results of a lifted turbulent H_2/N_2 jet flame in a vitiated coflow", *Proc. Combust. Inst.* 29: 1881–1888 (2002).

Scalar quantities obtained by post processing velocity fields measured by PIV using Chemical Reactor Networks.

Rishikesh Sampat* , Ferry Schrijer*, Arvind Gangoli Rao*
R.P.Sampat@tudelft.nl
*Faculty of Aerospace Engineering, TU Delft, Kluyverweg 1, 2629HS, Delft, The Netherlands

Abstract

Particle Image Velocimetry (PIV) is a technique used to measure the velocity fields in reacting flows by illuminating particles introduced as tracers in the flow. These measurements can be quite expensive in terms of time and effort due to the issue of window fouling by the particles under reacting flow conditions. Hence, it is useful to maximize the utility of this measurement. Typically one obtains information of velocity vectors, however, if the correct boundary conditions are known, the information may be further processed to obtain the chemical and thermodynamic state of the system. A similar concept of post processing PIV data has been adopted extensively in the literature to obtain pressure fields [1].

In this paper we explore this post-processing technique called PIV-CRN wherein the velocity vector field is post-processed to automatically generate an equivalent chemical reactor network (CRN) composed of 0D, perfectly stirred reactors. This is similar in ideology to the CFD-CRN method [2][3], wherein the flow field is obtained a priori through CFD (PIV in case of PIV-CRN), thereby allowing the use of detailed chemistry on the full domain to solve for species and temperature as a post-processing operation.

A synthetic velocity field is used to emulate the PIV data. In order to have a realistic velocity field that abides by the conservation equations as well as to have a relatively simple flow field, a 1D flamelet model in Cantera was used to generate it. It was a FreeFlame model with methane-air mixture at the inlet. The resultant flamelet grid was used to extract an equispaced grid with reduced number of points to better represent data that would be obtained by the interrogation window operation of the PIV algorithm from an image on a camera sensor. The vector field was used as a basis to generate a network of perfectly stirred reactors. Mass flow rates between reactors is determined by solving the steady state mass conservation equation, using the velocity field as input information to determine the relative flow between neighbouring reactors. The resultant Chemical Reactor Network is solved for conservation of species and energy using a detailed chemical mechanism, thereby giving distribution of temperature and species (scalars) in the domain

A good match with the 1D flamelet model in terms of ignition location and location of [OH]x[CH2O] peak was observed, which is considered a marker of heat release and hence the flame front [4]. The study is further extended to PIV measurements done on a laminar Bunsen flame. The velocity field is processed to obtain temperature and heat release rate distributions for a 2D field.

References

[1] B. W. Van Oudheusden, “PIV-based pressure measurement,” *Meas. Sci. Technol.*, vol. 24, no. 3, 2013.
[2] A. A. V. Perpignan, R. Sampat, and A. Gangoli Rao, “Modeling Pollutant Emissions of

Flameless Combustion With a Joint CFD and Chemical Reactor Network Approach," *Front. Mech. Eng.*, vol. 5, no. x, pp. 1–19, 2019.

[3] A. Cuoci, A. Frassoldati, A. Stagni, T. Faravelli, E. Ranzi, and G. Buzzi-Ferraris, "Numerical modeling of NOx formation in turbulent flames using a kinetic post-processing technique," *Energy and Fuels*, vol. 27, no. 2, pp. 1104–1122, 2013.

[4] R. L. Gordon, A. R. Masri, and E. Mastorakos, "Heat release rate as represented by [OH] × [CH 2 O] and its role in autoignition," vol. 7830, 2009.